Title

Loss of TET2 Affects Proliferation and Drug Sensitivity through Altered Dynamics of Cell-State Transitions

Journal

Cell Systems, 11(1)

ISSN

2405-4712

Authors

Morinishi, Leanna
Kochanowski, Karl
Levine, Ross L
et al.

Publication Date

2020-07-01

DOI

10.1016/j.cels.2020.06.003

Peer reviewed

HHS Public Access

Author manuscript

Cell Syst. Author manuscript; available in PMC 2021 July 22.

Published in final edited form as:

Cell Syst. 2020 July 22; 11(1): 86–94.e5. doi:10.1016/j.cels.2020.06.003.

Loss of TET2 affects proliferation and drug sensitivity through altered dynamics of cell-state transitions

Leanna Morinishi[1], **Karl Kochanowski**[2], **Ross L. Levine**[3,4,5], **Lani F. Wu**[2,*], **Steven J. Altschuler**[2,*,#]

[1]Bioinformatics Graduate Group, University of California, San Francisco, San Francisco, CA 94158, USA

[2]Department of Pharmaceutical Chemistry, University of California, San Francisco, San Francisco, CA 94158, USA

[3]Human Oncology and pathogenesis Program and Center for Hematologic Malignancies, Memorial Sloan Kettering Cancer Center, New York, NY 10065, USA

[4]Department of Medicine, Leukemia Service, Memorial Sloan Kettering Cancer Center, New York, NY 10065, USA

[5]Center for Epigenetics Research, Memorial Sloan Kettering Cancer Center, New York, NY 10065, USA

Summary

A persistent puzzle in cancer biology is how mutations, which neither alter growth signaling pathways nor directly interfere with drug mechanism, can still recur and persist in tumors. One example is the mutation of the DNA demethylase TET2 in acute myeloid leukemias (AMLs) that frequently persists from diagnosis through remission and relapse (Rothenberg-Thurley et al., 2018; Corces-Zimmerman et al., 2014; Nibourel et al., 2010), but whose fitness advantage in chemotherapy is unclear. Here we use isogenic human AML cell lines to show that TET2 loss-of-function alters the dynamics of transitions between differentiated and stem-like states. A conceptual mathematical model and experimental validation suggest these altered cell-state dynamics can benefit the cell population by slowing population decay during drug treatment and lowering the number of survivor cells needed to re-establish the initial population. These studies

[*]**Correspondence to** lani.wu@ucsf.edu and steven.altschuler@ucsf.edu.

Author contributions

Conceptualization and Methodology, L.M., K.K., S.J.A. and L.F.W.; Investigation, Analysis, and Visualization, L.M.; Resources, R.L.L.; Writing – Original Draft, L.M. and K.K.; Writing – Review & Editing, L.M., K.K., S.J.A. and L.F.W.; Supervision, K.K., R.L.L., S.J.A. and L.F.W.

[#]Lead Contact

Declaration of interests

RLL is on the Supervisory board of Qiagen, is on the SAB of Loxo (until 2019), Imago, Mana, Auron, Mission Bio, C4 Therapeutics and Isoplexis which include equity interest. He receives research support from and consulted for Celgene and Roche and consults for Incyte, Lilly, Janssen, Astellas, and Roche. He receives research support from Prelude. He has received honoraria from Astra Zeneca for an invited lecture and from Gilead for grant reviews.

shed light on the functional and phenotypic effects of a TET2 mutation in AML and illustrate how a single gene mutation can alter a cells' phenotypic plasticity. A record of this paper's Transparent Peer Review process is included in the Supplemental Information.

Graphical Abstract

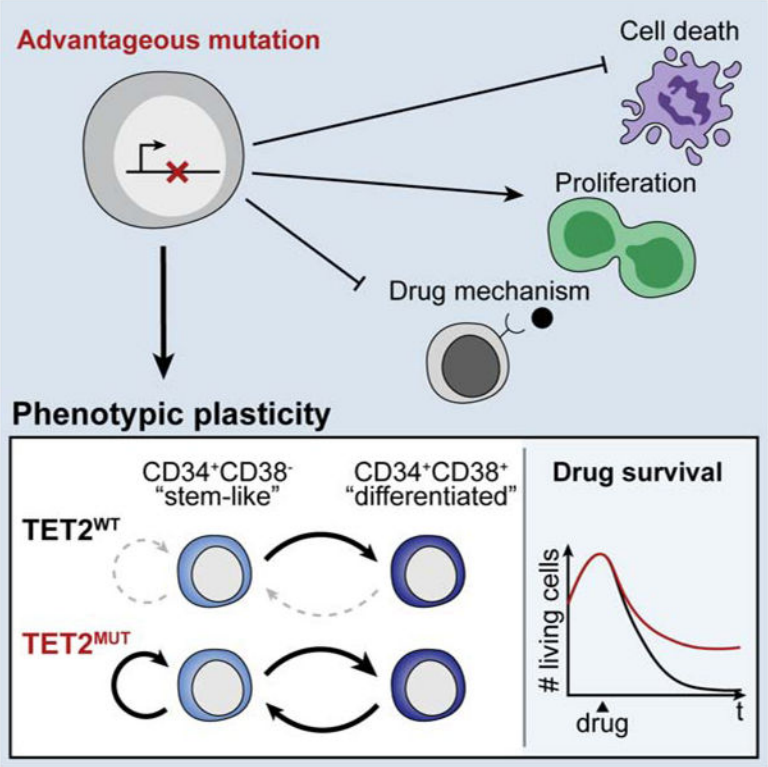

eTOC Blurb

Many recurrent mutations in cancer do not directly alter growth signaling or interfere with drug mechanism, yet are frequently observed in remission and relapse. Here we show that one such mutation in TET2, a commonly mutated epigenetic modifier in AML, can alter switching dynamics between stem-like and differentiated cell states, enhancing population fitness. This study illustrates how one mutation can alter phenotypic plasticity, and thereby provide an evolutionary strategy to promote cell population growth in and out of drug.

Introduction

A major challenge in cancer biology is to understand the function of recurrent mutations in the emergence of tumors or response to drug therapy. Some mutations clearly benefit cancer populations by altering regulation of growth signaling or programmed cell death (e.g. mutations in p53 or TGFβ signaling, Sanchez-Vega et al., 2018) or by directly interfering with drug effect (e.g. acquired EGFR T790M mutations in response to EGFR inhibitors, Ma, Wei and Song, 2011). However, for many observed mutations it is unclear how they affect either proliferation or drug resistance.

One example are mutations in the DNA demethylase TET2, found in ~15-20% of *de novo* AMLs (i.e. AMLs in patients with no clinical history of myelodysplastic syndrome (MDS) and no prior exposure to leukemogenic therapies; Cheson et al., 2003; Nibourel et al., 2010; Cancer Genome Atlas Research Network, 2013). Mutated TET2 is associated with pre-leukemic states such as clonal hematopoiesis (where a clone becomes overrepresented in the blood; Busque et al., 2012), and mutational persistence and adverse outcome in human AML (Corces-Zimmerman et al., 2014; Rothenberg-Thurley et al., 2018; Ding et al., 2012; Metzeler et al., 2011). However, due to its ability to alter DNA methylation genome-wide, the mechanisms by which TET2 mutation confers a benefit to AML cancer cell populations remain unclear. One possibility is that epigenetic variation in cancer cells increases phenotypic flexibility, enabling tumor evolution and progression (Feinberg et al., 2016; Flavahan et al., 2017). Indeed, recent studies have shown that loss of epigenetic effectors such as KDM5A in breast cancer (Hinohara et al., 2018) can affect drug sensitivity by enabling greater cell heterogeneity. Here we investigate whether TET2 loss similarly affects cell fitness in AML using an integrated approach of mathematical modeling and experimentation in paired WT and TET2-mutant isogenic human AML cell lines. We discover that TET2 mutation alters the dynamics of transitions between stem-like and differentiated cell states, enhancing population fitness in chemotherapy and lowering the number of cells needed to establish a cell population.

Results

TET2 loss-of-function mutation renders AML cell populations more stem-cell like

To investigate the consequences of TET2 mutation, we chose to compare isogenic human myeloblast cell lines expressing wildtype or mutant TET2 (Figure 1A). In human AMLs, TET2 is often found with truncating mutations or missense mutations in its catalytic domain resulting in TET2 loss-of-function (Hirsch et al., 2018; Smith et al., 2010). Therefore, isogenic cell lines were created by knocking out TET2 ($TET2^{KO}$) in two cell lines (KG1 and Thp1, see Methods). Methylation profiling confirmed that $TET2^{KO}$ has the expected effect on DNA methylation (Yamazaki et al., 2015; Asmar et al., 2013; Rasmussen et al., 2015): $TET2^{KO}$ cell lines display a significantly higher degree of hypermethylation compared to their WT counterparts ($TET2^{WT}$; t-test p-values KG1 <2.2e-16 and Thp1 2.9e-4; Figure 1B).

To gain an unbiased overview of the molecular changes induced by $TET2^{KO}$, we examined the transcriptomic and epigenomic profiles of the paired isogenic cell lines. RNAseq analysis identified ~300 similarly differentially expressed transcripts in both cell lines (fold-change>2, Supplemental Figure 1A, including reduced expression of myeloid differentiation markers (ITGAM, CORO1A, Wald test, BH adjusted p-values 9.99e-9 and 7.73e-2) and increased expression of markers associated with leukemic progenitors ($CD38^{-}$, $HLA\text{-}DRA^{-}$, TAL1, Wald test, BH adjusted p-values 3.83e-26, 1.74e-16, and 3.90e-7, Figure 1C, Supplemental Figure 1B; Chan et al., 2012; Nishioka et al., 2013; Vagapova et al., 2018). These data are consistent with analysis of TCGA LAML (phs000178.v1.p1) and OHSU (Tyner et al., 2018) datasets, which showed that TET2 expression is strongly correlated with genes expressed in the granulocytic lineage (Fisher's exact test adjusted p-values 6.27e-33 and 9.49e-20, Supplemental Tables 1-2, see Methods).

Differentially expressed genes in TET2^{KO} cells were found to be enriched for targets of RUNX1, a hematopoietic regulator known to promote stemness and myeloid fate decisions (Fisher's exact test adjusted p-value 7.76e-6, Supplemental Figure 1C, Supplemental Table 3; Ran et al., 2013). Consistently, the proximal promoter of RUNX1 was significantly differentially methylated in TET2^{KO} (Wald test, minimum adjusted p-value 1.22e-27, Supplemental Figure 1D) with a concomitant increase in the expression the RUNX1a isoform (Supplemental Figure 1E). Methylcellulose colony forming unit assays of TET2^{KO} cells also show increased numbers of colonies associated with oligopotent progenitor cells compared to TET2^{WT} controls (CFUGEMMs, Figure 1D, Supplemental Figure 1F). Overall, these data suggested that TET2^{KO} populations acquire more stem-like signatures, which was further validated by comparing their DNA methylation profiles to those of normal hematopoietic progenitors and leukemic stem cells (LSCs, Supplemental Figure 1G).

The TET2^{KO}-mediated acquisition of stem-like signatures was much more pronounced in KG1 than Thp1 in terms of expression profile and potential to form colonies of diverse myeloid lineages in methylcellulose assays (Figure 1D, Supplemental Figure 1F). This is presumably because the monocyte-like cells, Thp1, are already more differentiated than the myeloblast-like cells, KG1, regardless of TET2 mutational status. We therefore chose to focus on KG1 cells for the remainder of this work.

TET2 mutation changes dynamics of cell-state switching

To test whether this change in stem-like molecular signatures is caused by an increase in the fraction of cells with CD34^{hi}CD38^{lo} surface marker expression (a classic LSC-like profile; Costello *et al,* 2000; Gerber et al., 2012; Nishioka et al., 2013; Zeijlemaker et al., 2018) in TET2^{KO} compared to TET2^{WT} cells, we measured CD34 and CD38 surface marker expression in the KG1 population using flow cytometry. Quantification of CD34/CD38 expression revealed that the fraction of putatively stem-like CD34^{hi}CD38^{lo} cells was indeed increased in TET2^{KO} cell populations (Figure 2A, Supplemental Figure 2A).

To confirm that KG1 CD34^{hi}CD38^{lo} cells are more stem-like than CD34^{hi}CD38^{hi}, we fractionated TET2^{WT} and TET2^{KO} cells by CD38 expression and measured the expression of genes associated with hematopoietic differentiation. Consistent with bulk RNAseq data showing higher levels of pro-differentiation marker expression in TET2^{WT} cells compared to TET2^{KO} (Fig 1C), we found that differentiation markers increased with increasing levels of CD38 expression across both cell lines (trend seen for ITGAM, CORO1A, and TAL1, but not HOXA5; Supplemental Figure 2C). Further, growth rate decreased with increasing levels of CD38 expression (Supplemental Figure 2E) across KG1 TET2^{WT} and TET2^{KO} cells. Together, these data further support that KG1 CD34^{hi}CD38^{lo} cells are more stem-like and self-renewing, where CD34^{hi}CD38^{hi} cells are more differentiated and non-dividing.

How does TET2^{KO} alter the ratio between stem-like and differentiated cells? One possibility is that TET2^{KO} reduces the rate of differentiation. To test this, subpopulations of stem-like (*L*, CD34^{hi}CD38^{lo}) and differentiated (*H*, CD34^{hi}CD38^{hi}) cells were sorted in both TET2^{WT} and TET2^{KO} populations, and the ratio of *L* and *H* cells was monitored over time to steady-state (Figure 2D-E, Supplemental Figure 3B). Indeed, sorted stem-like *L* populations repopulated the differentiated state more slowly in TET2^{KO} (Figure 2D), and sorted TET2^{KO}

differentiated cell populations repopulated the stem-cell like state more rapidly than $TET2^{WT}$ (Figure 2E). These data suggest that $TET2^{KO}$ facilitates the reversible switching from differentiated to stem-like states in AML cells and provides intuition for why $TET2^{KO}$ has a larger fraction of stem-like cells in the population.

Mathematical modeling illustrates consequences of altered cell-state dynamics for survival of cell population

What are the functional consequences of having such altered cell-state dynamics, and in particular a higher fraction of stem-like cells? To address this question, we developed a simple mathematical model with two cell states (Figure 3, second panel): a stem-cell-like state L, and a more differentiated state H. This model is fully characterized by a linear, homogeneous system of ordinary differential equations (ODEs) with 6 parameters with values > 0 (see Methods). Parameters are denoted by: d_L and d_H, the death rates of the L and H states; g_L and g_H, the rates at which the L and H states proliferate; and r_{LH} and r_{HL}, the transition rates from L to H and H to L, respectively.

Using this model, we asked under which circumstances the observed altered cell-state dynamics – specifically an increased switch rate towards a stem-like state – would benefit a cell population. First, we focused on the impact of such altered cell-state dynamics during drug treatment (i.e. high death rates). In this case, the time to population collapse is dominated by the largest negative eigenvalue; the less negative the eigenvalue, the slower the population collapse. By computing the eigenvalues for the ODE, it can be seen that increasing the switch rate towards L slows population decay and "benefits" a drug-treated cancer population as long as:

$$(g_L - d_L) > (g_H - d_H) \qquad \text{(Inequality 1)}$$

This inequality simply compares net production rates (proliferation rate minus death rate) and requires it to be higher at L than H. In fact, while Inequality 1 is true, increasing r_{HL} or decreasing r_{LH} will slow population decay (Figure 3, first panel; see Methods) and thus "benefit" the cell population. This finding is in line with recent studies showing that cancer cells can reversibly transit between stem and differentiated states with different drug sensitivities (Jordan et al., 2016; Su et al., 2017; Gupta et al., 2011).

The same inequality also captures other cases in which switching to a stem-like state is either beneficial or detrimental (Figure 3, third and fourth panels). If cells rarely die, such as in a non-drug-treated condition ($d_L \approx 0$, $d_H \approx 0$) (**Case 1**), inequality 1 simplifies to

$$g_L > g_H$$

Here, switching to the L state (increasing r_{HL}) is beneficial for the cell population when the proliferation rate g_L of L is higher than the proliferation rate g_H of H, which is likely given the lower propensity of differentiated cells to divide. In this case, we expect cells carrying mutations that increase r_{HL} to take over the population. Conversely, if the differentiated cell

state H were protected from the adverse effects of drug treatment ($d_H \approx 0$) (**Case 2**), inequality 1 simplifies to

$$g_L - d_L > g_H$$

Here, increasing r_{HL} is only beneficial if the net production rate of L is larger than the proliferation rate g_H of H, which is unlikely for high doses of drug ($d_L \gg 0$). In this case, we expect cells carrying mutations that increase r_{HL} to be depleted from the population over time.

Overall, this conceptual mathematical model suggests that altered cell-state dynamics – specifically an increased switch rate towards a stem-like state – can indeed benefit the cell population both in presence or absence of drug treatment, as long as it falls within the parameter regime outlined by Inequality 1.

Experimental validation of modeling predictions

Does the TET2 mutation put the AML cancer population in this predicted advantageous parameter regime? Since the proliferation, death and switching rates cannot be disentangled directly from measurements, we estimated these rates by fitting our model to time course data of sorted TET2^{KO} and WT populations in the presence of cytosine arabinoside (AraC, a common first-line chemotherapy drug for AML; Figure 4B, Supplemental Figure 3B, see Methods). These parameter estimates confirmed that both KG1 TET2^{KO} and WT populations during drug treatment are in a regime where the net production of CD34^{hi}CD38^{lo} stem-like L cells outstrips that of CD34^{hi}CD38^{hi} differentiated H cells (as required by Inequality 1, Figure 4A-B). Therefore, switching to the stem-like state is more advantageous. As the TET2^{KO} populations have a higher r_{HL} switching rate and a lower r_{LH} switching rate, the model predicts that the TET2^{KO} population, as a whole, is more drug resistant. Indeed, drug treatment experiments confirmed that TET2^{KO} populations are less sensitive to AraC and doxorubicin than TET2^{WT} populations (Figure 4C, Supplemental Figure 3G). We also used the same experimental setup to determine model parameters for different drug conditions and different CD38-defined subpopulations (Supplemental Figure 3B,E, Figure 2). Our key results – Inequality 1 holds, TET2^{KO} cells have a higher transit rate r_{HL}, and TET2^{WT} cells have a higher rate r_{LH} – held true across experiments (Supplemental Figure 3J).

Further analysis of the model suggested two additional predictions. First, the model suggested that a population with a higher fraction of differentiated cell states will show reduced population survival in drug treatment (Figure 4D). To test this conjecture, two effectors known to enrich AML cell populations for the differentiated state (without altering cell death, Supplemental Figure 4C) were used: the inflammatory stimulus interferon gamma (IFNg) and the aldehyde dehydrogenase inhibitor disulfiram (DS; Amici et al., 2018; Xu et al., 2017). We confirmed that treatment with IFNg or DS enriched both TET2^{KO} and WT populations for the differentiated cell state after 72 hours of exposure (Figure 4E, Supplemental Figure 4A-B). Moreover, both effectors increased the efficacy of AraC treatment in both TET2^{KO} and WT populations, while several other effectors not known to

affect differentiation did not alter AraC sensitivity (Figure 4F, Supplemental Figure 4C, Supplemental Table 4).

Second, the model predicted that the increased ability of $TET2^{KO}$ to revert to a stem-like cell state (with higher proliferation potential) will result in improved $TET2^{KO}$ population outgrowth compared to $TET2^{WT}$ (Figure 4G). To test this prediction, we compared the number of colonies formed by $TET2^{KO}$ and $TET2^{WT}$ populations in methylcellulose assays, which assesses the ability of isolated cells to reform a colony (Figure 4H). As predicted, sorted stem-like cell populations showed increased cell colony numbers in both $TET2^{KO}$ and $TET2^{WT}$ populations. Moreover, unsorted $TET2^{KO}$ populations formed approximately 2x more colonies than their $TET2^{WT}$ counterparts (Figure 4I), highlighting their increased potential for population renewal. Thus, our results suggest that $TET2^{KO}$ populations not only have improved survival in the setting of therapeutic perturbations, but also have a higher likelihood to regrow an AML population from few surviving cells.

Discussion

Taken together, our results reveal that mutation of the epigenetic modifier TET2 in AML cells alters the transition dynamics between stem-like and differentiated cell states. These altered cell-state dynamics confer several benefits to the population in and out of drug, and provide a rationale for why the detection of TET2 mutants in patients in remission is strongly associated with a higher chance of relapse (Rothenberg-Thurley et al., 2018; Ding et al., 2012).

The key results from this study of a human CD34+CD38+ myeloid cell line (KG1) are consistent with past murine studies showing that TET2 mutation alters hematopoietic stem cell self-renewal and differentiation (Moran-Crusio et al., 2011). Future studies will be necessary to determine the generalizability of the cell state-switching phenomenon in other hematopoietic cell types and *in vivo.* Additionally, our study was limited to cell states defined by well-known surface markers. Incorporating powerful, unbiased approaches such as scRNAseq and analyses measuring RNA velocity (La Manno et al., 2018) could potentially uncover novel cell states and state switching dynamics that are relevant for drug survival.

An interesting question raised by this study is the degree to which the state switching rates are cell-intrinsic or extrinsically determined. In the process of confirming our model, we indeed found that the transition of $TET2^{KO}$ cells from $CD38^{hi}$ to $CD38^{lo}$ could be altered by effectors like DS and IFNg (Figure 4F). To characterize the extent to which cell-state switching rates are affected by signaling between the cells themselves, we grew KG1 $TET2^{WT}$ cells in media conditioned by $TET2^{KO}$ cells and *vice versa.* The distribution of CD38 expression in $TET2^{WT}$ cells was not affected by $TET2^{KO}$ conditioned media, but CD38 expression clearly increased for $TET2^{KO}$ cells grown in $TET2^{WT}$ conditioned media with decreased switching rates from $CD38^{hi}$ to $CD38^{lo}$ (Supplemental Figure 4D-F). Together, these results suggest that the switching rates of $TET2^{KO}$ cells can be influenced by external perturbations, while switching rates of $TET2^{WT}$ cells are more stable. Future studies will be needed to identify key soluble factors that distinguish $TET2^{KO}$ conditioned

media from TET2^{WT} and, more generally, to fully test the extent to which cell state switching rates are intrinsically determined.

This work provides further evidence that mutations which modulate switching rates between more and less drug-resistant states may provide an “evolutionary shortcut” to counteract the adverse effect of drug treatment (Jordan et al., 2016; Su et al., 2017; Gupta et al., 2011). The mechanisms driving this dynamic tumor heterogeneity will require deeper study, however, future therapeutic strategies incorporating this knowledge may better counteract tumor evolution in response to treatment. For example, a natural extension of the work presented here would be to use the model and understanding of cancer cell state switching dynamics to determine ideal dosing strategies (dosage, time course, pulsed administration, and so on) to help therapeutically manage patient outcomes. A recently published review made similar suggestions for future therapeutic development in melanoma (Bai et al., 2019).

Our results have implications for AML mutations beyond TET2: the conceptual mathematical model shows that as long as stem-like and differentiated cell states differ in their net production during drug treatment (i.e., Inequality 1 is fulfilled), any other mutation increasing the transition rate towards the stem-like state will be beneficial as well. Thus, we conjecture that mutations in other epigenetic modifiers might confer a fitness advantage to drug-treated AML populations through similar mechanisms. In cancer, the target space for mutations that directly interfere with drug function is likely smaller than the target space for dysregulation of cell states; this is known to be the case in bacteria, where the number of genes conferring increased antibiotic tolerance far exceeds the number of genes conferring drug resistance (Girgis, Harris, and Tavazoie, 2012; Brauner et al., 2016). Future studies characterizing cell states and transition dynamics will provide new insight into why certain mutations are selected for, and persist in, cancer, and may lead to new approaches which increase the efficacy of current cancer therapies.

Key Changes Prompted by Reviewer Comments

The manuscript was extended with supplemental figures showing the robustness of switching parameters to CD38 expression, the biological significance of CD38-defined subpopulations, and the effect of conditioned media on cell-state switching. An experiment showing sorted subpopulations returning to steady-state is now highlighted in Figure 2C-E. Figure legends and the Methods section were expanded and clarified extensively, especially those pertaining to the selection of the CD38 threshold and the range of fit parameters. The Introduction was revised to include more literary context. The Discussion section was expanded to include further limitations of our study and potential future directions in therapeutically managing patient outcome. For context, the complete Transparent Peer Review Record is included within the Supplemental Information.

STAR Methods

Resource availability

Lead Contacts—Further information and requests for resources and reagents should be directed to and will be fulfilled by Steven J. Altschuler (steven.altschuler@ucsf.edu).

Materials Availability—This study did not generate new unique reagents.

Data and Code Availability—The RNA sequencing, DNA methylation, and flow cytometry datasets generated during this study along with original code to generate all figures are available at doi:10.17632/xmvz47rpg6.1. All original code to generate parameter fits or run the Gillespie algorithm is freely available for download at https://github.com/AltschulerWu-Lab/tet2-dynamics.

Experimental Model and Subject Details

KG1 (RRID: CVCL_0374; male) and Thp1/Thp1 TET2^{KD} (RRID: CVCL_0006; male) cells were generous gifts from the Shannon lab at UCSF and Levine lab at MSKCC, respectively. Cells were cultured in ATCC-recommended media and incubated at 37°C with 5% CO_2. All cell lines were maintained in 75ml or 250ml Suspension Culture flasks (CellTreat, Pepperell, MA) between 0.5e6 and 1e6 cells/ml.

Method Details

Generating TET2 mutants—The AML cell lines KG1 and Thp1 were selected as they express wildtype TET2 but do not express mutant FLT3, which is known to have synergistic epigenetic effects (Kunimoto et al., 2018, Shish *et al.*, 2015). To make TET2^{KO} cells in the KG1 cell line, guides targeting exon 3 of TET2 (an exon with frequent indel mutations in patients with MDS; Smith et al., 2010) were designed in Benchling (5'-CACCGAGGCCAATTAAGGTGGAACC-3'). pSpCas9(BB)-2A-Puro (PX459) V2.0 was a gift from Feng Zhang (Addgene plasmid #62988). Guides were cloned into PX459 using Bbsl sites, and vectors transfected into KG1 cells with the Cell Line Nucleofector Kit R (Lonza Group, Basel, Switzerland) with protocol V-001 and according to the manufacturer's protocol. After 48h, FITC-positive cells were isolated via FACS and expanded for 10 days. The TET2 mutation created a frameshift mutation causing truncation upstream of the conserved catalytic domain of TET2, consistent with tumors observed in patients (Weissman et al., 2012).

Drug and effector treatment—Prior to addition to cell culture media, Cytosine Beta-D-Arabinofuranoside (Sigma-Aldrich, St. Louis, MO) and 2-Deoxy-D-glucose (Sigma-Aldrich) were dissolved in H_2O, CCCP (Sigma-Aldrich), Disulfiram (Sigma-Aldrich), Etacrynic acid (Sigma-Aldrich), and Torin1 (Cell Signaling Technology, Danvers, Massachusetts) were dissolved in DMSO, and IFNg (Peprotech, Rocky Hill, NJ) was dissolved in culture media to 1000x the desired final concentration. Final DMSO (or other diluent) concentration was always 0.1%.

Cell-state transition model—We modeled a cell system with $\boldsymbol{m}$ states as a linear, homogenous system of ODEs. In matrix form this is written as

$$\frac{d\boldsymbol{v}}{dt} = \boldsymbol{M}\boldsymbol{v}$$

where $\boldsymbol{v}$ is cell-state vector of length $\boldsymbol{m}$, and $\boldsymbol{M}$ is a $\boldsymbol{m}$ x $\boldsymbol{m}$ matrix representing cell-state transitions. We do not assume the matrix $\boldsymbol{M}$ is stochastic, which allows expansion or contraction of the total number of cells in the system—reflecting cell division or drug sensitivity—to occur. In our study, we considered two states: $\boldsymbol{L}$ (CD38^{lo}) or $\boldsymbol{H}$ (CD38^{hi}):

$$\frac{d}{dt}\begin{bmatrix} L \\ H \end{bmatrix} = \begin{bmatrix} (g_L - r_{LH} - d_L) & r_{HL} \\ r_{LH} & (g_H - r_{HL} - d_H) \end{bmatrix} \begin{bmatrix} L \\ H \end{bmatrix}$$

Where g_L and g_H are the growth rates and d_L and d_H the death rates of cell-states $\boldsymbol{L}$ and $\boldsymbol{H}$, respectively. Here, r_{LH} is the transition rate from $\boldsymbol{L}$ to $\boldsymbol{H}$, and r_{HL} is the transition rate from $\boldsymbol{H}$ to $\boldsymbol{L}$. All matrix parameters are considered to be real, non-negative numbers. If we define

$$\alpha = -g_L + r_{LH} + r_{HL} - g_H + d_L + d_H$$
$$\beta = \sqrt{\alpha^2 + 4r_{LH}(g_H - d_H) + 4r_{HL}(g_L - d_L) + 4(g_H d_L + g_L d_H) - 4(g_L g_H + d_L d_H)}$$

then the eigenvalues of $\boldsymbol{M}$ are

$$\lambda_1 = \frac{1}{2}(-\alpha - \beta)$$

$$\lambda_2 = \frac{1}{2}(-\alpha + \beta)$$

with eigenvectors

$$\overrightarrow{v_1} = \begin{bmatrix} -\dfrac{-g_L + r_{LH} - r_{HL} + g_H + d_L - d_H + \beta}{2r_{HL}} \\ 1 \end{bmatrix}$$
$$\overrightarrow{v_2} = \begin{bmatrix} -\dfrac{-g_L + r_{LH} - r_{HL} + g_H + d_L - d_H + \beta}{2r_{HL}} \\ 1 \end{bmatrix}$$

For convenience, we define the difference in production between the two states

$$P \equiv (g_L - d_L) - (g_H - d_H)$$

To find the regime where changing r_{HL} (asympototically) increases survival rate, we focus on the larger of the other two eigenvalues, namely $\boldsymbol{\lambda_2}$. Taking the derivative of $\boldsymbol{\lambda_2}$ with respect to the state-switching parameters gives:

$$\frac{d\lambda_2}{dr_{HL}} = \frac{1}{2}\left(\frac{r_{LH} + r_{HL} + P}{\beta} - 1\right)$$
$$\frac{d\lambda_2}{dr_{LH}} = \frac{1}{2}\left(\frac{r_{LH} + r_{HL} + P}{\beta} - 1\right)$$

Using Wolfram|Alpha, we find: a) $\frac{d\lambda_2}{dr_{HL}} > 0$ holds if $P > 0$ and $r_{HL} > -(\sqrt{r_{LH}} - \sqrt{P})^2$; and b) $\frac{d\lambda_2}{dr_{LH}} \leq 0$ holds if either (i) $P > 0$, $0 \leq r_{LH} < P$, and $r_{HL} > -(\sqrt{r_{LH}} - \sqrt{P})^2$, or if (ii) $P > 0$ and $r_{LH} \geq P$. In our model, we only consider non-negative, real-valued parameter values. Thus, as long as the inequality $P > 0$ holds, $\frac{d\lambda_2}{dr_{HL}} > 0$ and $\frac{d\lambda_2}{dr_{LH}} \leq 0$.

A two-state system with constant switching rates can equilibrate to a constant fraction of states (a steady state) provided the cell population does not rapidly crash. This is possible because flux into and out of each state can be balanced, and is why observations such as Figure 2D (where TET2^{KO} cells appear to not switch and instead retain a stem-like state) can still be an accurate reflection of cells in constant flux. However, cell proliferation, death, and switching rates cannot be disentangled directly from bulk measurements. Therefore, we estimated these rates by fitting our model to time course data of sorted TET2^{KO} and WT populations. To find best fit parameters for this system, cell-state compositions from the flow cytometry experiments shown in Supplemental Figure 3B & E or Figure 2D-E (using data from both CD38^{hi}- and CD38^{lo}-sorted subpopulations, described below) were used as input into the model. Prediction error (the sum of the differences between the predicted and measured number of cells in each cell-state at each timepoint) was minimized with fminsearch in MATLAB (version R2019a) with MaxIter of 5000. To eliminate “solutions” that did not converge or had poor fit, prediction error for 1000 sets of random parameter values was calculated to form a null distribution for each condition, and the 0.005-quantile for this null distribution was used as an upper limit for reasonable error values (Supplemental Figure 3H). To establish the probable range of transition parameters, best-fit parameters for 1000 random initializations (x0 in the fminsearch function) were found and plotted (Supplemental Figure 3I). Representative values for fit parameters for KG1 TET2^{WT} and TET2^{KO} cells are shown in Figure 4A. Median values for fit parameters or fit parameter ratios from converged solutions are shown in Supplemental Figure 3J and Supplemental Figure 4F.

Solving the matrix ODE gave

$$\begin{bmatrix} L \\ H \end{bmatrix} = \begin{bmatrix} \vec{v}_1^{\,1} & \vec{v}_1^{\,2} \\ \vec{v}_2^{\,1} & \vec{v}_2^{\,2} \end{bmatrix} \begin{bmatrix} Ae^{\lambda_1 t} \\ Be^{\lambda_2 t} \end{bmatrix} \tag{12}$$

After solving for the constants $\boldsymbol{A}$ and $\boldsymbol{B}$, model predictions were made using representative best fit parameters and initial conditions observed in the experiment (e.g. number of CD38^{hi} and CD38^{lo} cells in day 0 sorted cell populations; method for calling CD38$^{lo/hi}$ described below).

For colony forming simulations, 100 colonies were “seeded” with 10 individual cells as colony founders with 50% in the $\boldsymbol{L}$ state and 50% in $\boldsymbol{H}$ unless otherwise noted. To simulate growth without drug treatment, rates were estimated by fitting the model to flow cytometry experimental data (described below) without AraC treatment. The Gillespie algorithm was

implemented to find the number of cells in the ***L*** or ***H*** states at time ***t***. Cells "grew" for 10 time-steps before the number of cells in each colony was counted. Colonies with more than 100 cells were considered "grown out".

DNA methylation profiling—DNA methylation was profiled using Illumina's Infinium MethylationEPIC BeadChip (Illumina, San Diego, CA). DNA of technical replicates for each condition was extracted using the Zymo Quick-DNA kit (Zymo Research, Irvine, CA, KG1 n=6 per condition, Thp1 n=2 per condition). Bisulfite conversion, nanodrop quantitation, array scanning, and normalization was performed by the Vincent J. Coates Genomics Sequencing Laboratory at UC Berkeley.

mRNA-seq—RNA extraction of technical replicates was performed using the Lexogen SPLIT RNA extraction kit (Lexogen, Vienna, Austria, n=6 per condition), and libraries were prepared using the QuantSeq 3' mRNA-Seq Library Prep Kit FWD for Illumina. Samples were quantified with Invitrogen Qubit (Invitrogen, Carlsbad, CA) prior to pooling, and library size and integrity was confirmed using the Agilent Bioanalyzer with the high-sensitivity DNA kit (Agilent, Santa Clara, CA). RNA sequencing was performed using 50bp single-end sequencing on the Illumina HiSeq 4000 in the Center for Advanced Technology at UC San Francisco. A PhiX control library was used as an in-run control, spiked in at 5%.

Immunofluorescence for flow cytometry—Cells were pelleted and washed with wash buffer (HBSS + 1% BSA, filtered with a 50ml Steriflip unit (Millipore, Burlington, MA)) prior to 30m incubation in Fc Receptor Blocker (Innovex Biosciences, Richmond, CA) on ice in the dark. Cells were washed twice before resuspension in wash buffer containing conjugated antibodies for flow cytometry at their recommended concentrations (CD34-PE 555822, CD38-PE-Cy5 555461, Becton Dickinson, Franklin Lakes, NJ), and incubation for 30m on ice in the dark. Cells were washed three times and resuspended in 350uL wash buffer before measurement with flow cytometry at a flow rate of 9.0. Doublets were called based on gates drawn for FSC-A and FSC-W, and dead cells were counted based on gates drawn in FSC-A and SSC-A. All flow cytometry or FACS was performed on the Aria IIu in the Center for Advanced Technologies at UC San Francisco.

External marker tracking by flow cytometry—For Figure 2 and Supplemental Figure 3B-C, equal numbers of $CD38^{hi}$ and $CD38^{lo}$ subpopulations of $TET2^{WT}$ and $TET2^{KO}$ cells were isolated by FACS (gate in Figure 2A, set such that <0.5% of unstained cells would be counted as $CD38^{hi}$; see Supplemental Figure 2A) and seeded separately in a round-bottom 96-well plate (CELLSTAR) at 1e5 cells/ml. For Supplemental Figure 3E-F, equal numbers of cells from the "tails" (bottom/top 5%) of the CD38 distributions of stained, unsorted $TET2^{WT}$ and $TET2^{KO}$ cells (see Supplemental Figure 3D) were isolated by FACS and seeded separately in a round-bottom 96-well plate (CELLSTAR) at 1e5 cells/ml. For day 0 timepoints, aliquots of freshly sorted cells were reflowed and recorded. For Supplemental Figure 3A-C, cells were treated with 0, 1, or 4uM AraC in technical triplicates. No drug was applied to the technical replicates shown in Figure 2C and Supplemental Figures 3D-F. Plates were covered with Breathe-Easy sealing membranes (Sigma-Aldrich) before incubation. For longer timepoints, media (with or without drug, as relevant) was exchanged

every 3 days. At each timepoint, all cells in each replicate well were washed and stained for CD34 and CD38 (described above) and re-profiled by flow cytometry. To account for day-to-day variations in Aria IIu laser power or other settings, raw fluorescence intensity for each channel was normalized by the median intensity of unsorted, unstained controls of the appropriate cell line for each timepoint prior to analysis. For all experiments, $CD38^{hi}$ and $CD38^{lo}$ cell counts for analysis and model-fitting were called based on the same sorting threshold shown in Figure 2A (see Supplemental Figure 2A). The number of living cells in each cell state served as input to the model to fit parameters for the cell-state transition matrix in both cell lines for both treated and untreated conditions (described above).

Methylcellulose colony forming unit assay—Cells were counted with the TC20 automatic cell counter (Bio-Rad) with Trypan blue prior to plating in triplicate as technical replicates in MethoCult H4034 Optimum (Stemcell Technologies, Vancouver, CAN) in 35mm cell culture dishes (Eppendorf, Hamburg, DE) according to the manufacturer's instructions. Cells were incubated for 2 weeks at 37°C with 5% CO_2. To maintain humidity, 4 MethoCult dishes were incubated amongst three lidless 35mm dishes each filled with 3ml sterile ddH_2O inside a 150mm glass petri dish with a lid (Corning, Corning, NY). Water was replenished every 3 days. Colonies were enumerated according to the manufacturer's instructions. Results shown are representative results from two independent experiments.

Cell viability assays—For sorted population growth or effector viability assays (Supplemental Figures 2E & 4C), $TET2^{WT}$ and $TET2^{KO}$ cells were stained for CD34 and CD38 (described above) and segregated by CD38 expression with FACS as shown (Supplemental Figure 2D and Figure 2A, respectively). For day 0 timepoints, aliquots of freshly sorted cells were reflowed and recorded. Sorted cells were plated in round-bottom 96-well plates (CELLSTAR, Dallas, TX) at 1e5 cells/ml with replicates for each timepoint. For treated conditions, AraC and effectors were diluted and added as described above. Plates were covered with Breathe-Easy sealing membranes (Sigma-Aldrich) before incubation at 37°C with 5% CO_2. For longer timepoints, media (with or without drug, as relevant) was exchanged every 3 days. At each timepoint, all cells in each replicate well were washed, stained, and measured with the Aria IIu for the first 2000 events. The density of living cells (# of cells per ml, Supplemental Figure 2E) was calculated as the number of living cells observed per sample divided by the total length of time the sample took to reach 2000 events, and divided by the flow rate (~90 uL/minute for flow rate 9.0 on the Aria IIu).

For drug viability assays (Figure 4C, Supplemental Figure 3G), cells were plated as technical replicates at 1e5 cells/ml and treated with drug for 72h. For readout, plates were allowed to cool to room temperature before combining well-mixed cells and cell media 1:1 with room temperature CellTitre-Glo 2.0 (Promega, Madison, WI) in opaque white tissue culture plates (Corning). Reactions were allowed to proceed according to the manufacturer's protocol, and luminescence was read out with the Biotek H4 plate reader (BioTek, Winooski, VT) in the Center for Advanced Technology at UC San Francisco. Results shown are representative results from three independent experiments.

RT-qPCR and PCR—For measuring TET2 expression, RNA was extracted from three technical replicates with the Direct-zol RNA Miniprep kit (Zymo Research) according to

manufacturer's instructions with TRI Reagent (Thermo Fisher Scientific, Waltham, MA). For measuring CD38, ITGAM, CORO1A, TAL1, and HOXA5 expression, cells were stained for CD34 and CD38 (described above) and fractionated by CD38 expression via FACS (gates shown in Supplemental Figure 2B). RNA was extracted from sorted cells (2 replicates of 300k cells) with the RNeasy Plus Mini Kit (QIAGEN, Hilden, DE) according to manufacturer's instructions. Reverse transcription with iScript Reverse Transcription Supermix (Bio-Rad, Hercules, CA) was followed by qPCR with DyNAmo Flash SYBR Green qPCR kit (Thermo Fisher Scientific) according to the recommended protocol on the BioRad CFX Connect in the Center for Advanced Technologies at UC San Francisco. The set of genes measured was composed of genes of interest from the bulk RNAseq experiment (Supplemental Figure 1B) and relevant gene sets in the literature (GSEA: gal_leukemic_stem_cell (Gal et al., 2006), gentles_leukemic_stem_cell (Gentles et al., 2010), eppert_ce_hsc_lsc (Eppert et al., 2011)). Primers were obtained from IDT (San Jose, CA). Primer sequences for human RUNX1, TET2, HOXA5, and GAPDH were as previously described (Fujita et al., 2001; Cimmino et al., 2017; McLaughlin-Drubin et al., 2011). Primer sequences for CD38, CORO1A, ITGAM, and TAL1 were generated with the Primer Design Tool in Benchling.

Quantification and Statistical Analysis

Differential RNA expression analysis—mRNA reads were mapped and counted using the Integrated QuantSeq data analysis pipeline on Bluebee Platform (Bluebee, Rijswijk, Netherlands). Briefly, reads were trimmed with BBDuk, aligned to human GRCh38 with STAR, and counted with HTSeq-count. Gene filtering and differential expression analysis was performed in R (version 3.6.0; R Core Team, 2019). Genes were filtered by count such that all genes had 3 or more samples with 10 or more counts. Differential expression analysis was then performed using DESeq2 (version 1.24, Love et al., 2014) on gene counts. Genes that were found to be significantly differentially expressed (N=6 technical replicates; Wald test, BH adjusted p-value < 0.05) with an absolute Log_2fold-change in expression > 1.5X in a paired analysis of untreated cell lines were submitted to Enrichr (Kuleshov et al., 2016) for enrichment analysis. Statistical details can be found in the Results section and legends for Figure 1 and Supplemental Figure 1.

Differential DNA methylation analysis—Differential methylation analysis was performed with ChAMP (package version 2.14.0, Tian et al., 2017) in R (version 3.6.0; R Core Team, 2019). Significantly differentially methylated regions (KG1 n=6, Thp1 n=2 technical replicates per condition; Wald test, BH adjusted p-value < 0.05) were found with DMRcate (version 1.20, Peters et al., 2015), and visualization done with Gviz (version 1.28, Hahne et al., 2016). Statistical details can be found in the Results section and legend for Supplemental Figure 1.

Methylation age and stemness profiles—Quantile normalized values from the aforementioned ChAMP analysis were used as input to the DNA methylation age calculator in R as per the tutorial (horvath.genetics.ucla.edu) (Horvath, 2013). For visualization purposes, results for $TET2^{WT}$ and $TET2^{KO}$ cells were normalized to $TET2^{wt}$.

For the “stem-like” epigenetic signatures, we used a publicly available dataset of DNA methylation profiles from normal hematopoietic progenitors and leukemic cells sorted by CD34/CD38 expression (GEO: GSE63409; Jung et al., 2015). Linear discriminant analysis (LDA) was applied using the MASS package (version 7.3-51.4, Venables et al., 2002) in R to identify an optimal transform that increased separation of DNA methylation profiles across three key reference populations: normal HSCs, $CD34^{+}CD38^{-}$ putative LSCs, and $CD34^{-}$ leukemia cells. The rest of the public dataset, as well as methylation data from the paired $TET2^{wt/TET2^{ko}}$ cell lines, was projected into the lower-dimensional LDA space.

TET2 expression analysis—Expression profiles for the following datasets were queried from the Cancer Genomics Data Server (CGDS) using cdgsr (version 1.3.0, Cerami et al., 2012). Our results are, in part, based upon data generated by The Cancer Genome Atlas managed by the NCI and NHGRI. Information about TCGA can be found at http://cancergenome.nih.gov. For the datasets TCGA-LAML (dbGaP accession phs000178.v1.p1) and AML-OHSU (Tyner et al., 2018), genes with coefficient of variation < 0.1 across samples were dropped from subsequent analysis. Pearson correlation calculations were performed in R (version 3.6.0). Genes with expression that strongly correlated (cor > 0.45) or anti-correlated (cor < −0.45) with TET2 expression were submitted to Enrichr (Kuleshov et al., 2016) for enrichment analysis. Statistical details can be found in the Results section corresponding to Supplemental Tables 1-2.

Supplementary Material

Refer to Web version on PubMed Central for supplementary material.

Acknowledgments

Thanks to Kevin Shannon, Ben Huang, Dylan Altschuler, Jason Altschuler, Jake Bieber, Jeremy Chang, Louise Heinrich, Weiyue Ji, Capria Rinaldi, Xiaoxiao Sun, Alex Marson, and Michael McManus for helpful discussions and feedback. Funding sources: L.M. is supported by NSF GRFP; K.K. is supported by the European Molecular Biology Organization (long-term fellowship ALTF 1167–2016) and the Swiss National Science Foundation; R.L.L. is supported by National Cancer Institute grants P01 CA108671 and R35197594 as well as a Leukemia & Lymphoma Society Specialized Center of Research grant; L.F.W. is supported by NCI-NIH RO1 CA185404 & CA184984; and S.J.A. is supported by GM112690, NSF PHY-1545915 and SU2C/MSKCC 2015-003. This study was supported in part by HDFCCC Laboratory for Cell Analysis Shared Resource Facility through a grant from NIH (P30CA082103).

References

Amici SA, Young NA, Narvaez-Miranda J, Jablonski KA, Arcos J, Rosas L, Papenfuss TL, Torrelles JB, Jarjour WN, and Guerau-de-Arellano M (2018). CD38 Is Robustly Induced in Human Macrophages and Monocytes in Inflammatory Conditions. Frontiers in immunology, 9, 1593. [PubMed: 30042766]

Asmar F, Punj V, Christensen J, Pedersen MT, Nielsen AB, Hother C, Ralfkiaer U, Brown P, Ralfkiaer E, Helin K, and Grønbk K (2013). Genome-wide profiling identifies a DNA methylation signature that associates with Tet2 mutations in diffuse large B-cell lymphoma. Haematologica, 98(12), 1912–1920. [PubMed: 23831920]

Bai X, Fisher DE, Flaherty KT (2019). Cell-state dynamics and therapeutic resistance in melanoma from the perspective of MITF and IFNg pathways. Nature Reviews Clinical Oncology, 16, 549–562.

Brauner A, Fridman O, Gefen O, Balaban NQ (2016). Distinguishing between resistance, tolerance and persistence to antibiotic treatment. Nature Reviews Microbiology, 14(5), 320–330. [PubMed: 27080241]

Busque L, Patel J, Figueroa M, et al. (2012). Recurrent somatic TET2 mutations in normal elderly individuals with clonal hematopoiesis. Nature Genetics 44, 1179–1181. [PubMed: 23001125]

Cancer Genome Atlas Research Network. (2013). Genomic and epigenomic landscapes of adult de novo acute myeloid leukemia. The New England Journal of Medicine, 368(22), 2059–2074. [PubMed: 23634996]

Cerami E, Gao J, Dogrusoz U, Gross BE, Sumer SO, Aksoy BA, Jacobsen A, Byrne CJ, Heuer ML, Larsson E, et al. (2012). The cBio Cancer Genomics Portal: An Open Platform for Exploring Multidimensional Cancer Genomics Data. Cancer Discovery, 2(5), 401–404. [PubMed: 22588877]

Chan KT, Creed SJ, & Bear JE (2012). Coronin family of actin regulators. 21(8), 481–488.

Cheson BD, Bennett JM, Kopecky KJ, Buchner T, Willman CL, Estey EH, Schiffer CA, Doehner H, Tallman MS, Lister TA, et al. (2003). Revised recommendations of the International Working Group for Diagnosis, Standardization of Response Criteria, Treatment Outcomes, and Reporting Standards for Therapeutic Trials in Acute Myeloid Leukemia. Journal of Clinical Oncology, 21(24), 4642–4649. [PubMed: 14673054]

Cimmino L, Dolgalev I, Wang Y, Yoshimi A, Martin GH, Wang J, Ng V, Xia B, Witkowski MT, Mitchell-flack M, et al. (2017). Restoration of TET2 Function Blocks Aberrant Self-Renewal and Leukemia Progression. Cell, 170(6), 1079–1095. [PubMed: 28823558]

Corces-Zimmerman MR, Hong WJ, Weissman IL, Medeiros BC, Majeti R (2014). Preleukemic mutations in human acute myeloid leukemia affect epigenetic regulators and persist in remission. Proceedings of the National Academy of Sciences of the United States of America, 111 (7), 2548–2553. [PubMed: 24550281]

Costello RT, Mallet F, Gaugler B, Sainty D, Arnoulet C, Gastaut J, Olive D (2000). Human acute myeloid leukemia $CD34^{+}CD38^{-}$ progenitor cells have decreased sensitivity to chemotherapy and Fas-induced apoptosis, reduced immunogenicity, and impaired dendritic cell transformation capacities. Cancer Research, 60(16), 4403–4411. [PubMed: 10969785]

Ding L, Ley TJ, Larson DE, Miller CA, Koboldt DC, Welch JS, Ritchey JK, Young MA, Lamprecht T, McLellan MD, et al. (2012). Clonal evolution in relapsed acute myeloid leukaemia revealed by whole-genome sequencing. Nature, 481(7382), 506–510. [PubMed: 22237025]

Eppert K, Takenaka K, Lechman ER, Waldron L, Nilsson B, van Galen P, Metzeler KH, Poeppl A, Ling V, Beyene J, et al. (2011). Stem cell gene expression programs influence clinical outcome in human leukemia. Nature Medicine, 17(9), 1086–93.

Feinberg AP, Koldobskiy MA, Göndör A (2016). Epigenetic modulators, modifiers and mediators in cancer aetiology and progression. Nature Reviews Genetics, 17, 284–299.

Flavahan WA, Gaskell E, Bernstein BE (2017). Epigenetic plasticity and the hallmarks of cancer. Science, 357(6348),

Fujita Y, Nishimura M, Taniwaki M, Abe T, Okuda T (2001). Identification of an alternatively spliced form of the mouse AML1/RUNX1 gene transcript AML1c and its expression in early hematopoietic development. Biochemical and Biophysical Research Communications, 281(5), 1248–1255. [PubMed: 11243869]

Gal H, Amariglio N, Trakhtenbrot L, Jacob-Hirsh J, Margalit O, Avigdor A, Nagler A, Tavor S, Ein-Dor L, Lapidot T, et al. (2006). Gene expression profiles of AML derived stem cells; similarity to hematopoietic stem cells. Leukemia, 20(12), 2147–54. [PubMed: 17039238]

Gentles AJ, Plevritis SK, Majeti R, Alizadeh AA (2010). Association of a leukemic stem cell gene expression signature with clinical outcomes in acute myeloid leukemia. JAMA, 304(24), 2706–2715. [PubMed: 21177505]

Gerber JM, Smith BD, Ngwang B, Zhang H, Vala MS, Morsberger L, Galkin S, Collector MI, Perkins B, Levis MJ, et al. (2012). A clinically relevant population of leukemic CD34+$CD38^{-}$ cells in acute myeloid leukemia. Blood, 119(15), 3571–3577. [PubMed: 22262762]

Girgis HS, Harris K and Tavazoie S (2012). Large mutational target size for rapid emergence of bacterial persistence. Proceedings of the National Academy of Sciences of the United States of America, 109(31), 12740–12745. [PubMed: 22802628]

Gupta PB, Fillmore CM, Jiang G, Shapira SD, Tao K, Kuperwasser C, Lander ES (2011). Stochastic state transitions give rise to phenotypic equilibrium in populations of cancer cells. Cell, 146(4), 633–644. [PubMed: 21854987]

Hahne F & Ivanek R (2016). Statistical Genomics: Methods and Protocols In Visualizing Genomic Data Using Gviz and Bioconductor (335–351). Springer New York.

Hinohara K, Wu HJ, Vigneau S, McDonald TO, Igarashi KJ, Yamamoto KN, Madsen T, Fassl A, Egri SB, Papanastasiou M, et al. (2018). KDM5 histone demethylase activity links cellular transcriptomic heterogeneity to therapeutic resistance. Cancer Cell, 34(6), 939–953.e9. [PubMed: 30472020]

Hirsch CM, Nazha A, Kneen K, Abazeed ME, Meggendorfer M, Przychodzen BP, Nadarajah N, Adema V, Nagata Y, Goyal A, et al. (2018). Consequences of mutant Tet2 on clonality and subclonal hierarchy. Leukemia, 32(8), 1751–1761. [PubMed: 29795413]

Horvath S (2013). DNA methylation age of human tissues and cell types. Genome Biology, R115. [PubMed: 24138928]

Jordan NV, Bardia A, Wittner BS, Benes C, Ligorio M, Zheng Y, Yu M, Sundaresan TK, Licausi JA, Desai R, et al. (2016). HER2 expression identifies dynamic functional states within circulating breast cancer cells. Nature, 537(7618), 102–106. [PubMed: 27556950]

Jung N, Dai B, Gentles AJ, Majeti R, and Feinberg AP (2015). An LSC epigenetic signature is largely mutation independent and implicates the HOXA cluster in AML pathogenesis. Nature Communications, 6, 8489.

Kuleshov MV, Jones MR, Rouillard AD, Fernandez NF, Duan Q, Wang Z, Koplev S, Jenkins SL, Jagodnik KM, Lachmann A, et al. (2016). Enrichr: a comprehensive gene set enrichment analysis web server 2016 update. Nucleic Acids Research, 44(W1), W90–7. [PubMed: 27141961]

Kunimoto H, Meydan C, Nazir A, Whitfield J, Shank K, Rapaport F, Maher R, Pronier E, Meyer SC, Garrett-Bakelman FE, et al. (2018). Cooperative Epigenetic Remodeling by Tet2 Loss and NRAS Mutation Drives Myeloid Transformation and MEK Inhibitor Sensitivity. Cancer Cell, 33(1), 44–59.e8. [PubMed: 29275866]

La Manno G, Soldatov R, Zeisel A, Braun E, Hochgerner H, Petukhov V, Lidschreiber K, Kastriti ME, Lonnerberg P, Furlan A, et al. (2018). RNA velocity of single cells. Nature, 560(7719), 494–498. [PubMed: 30089906]

Love MI, Huber W, Anders S (2014). Moderated Estimation of Fold Change and Dispersion for RNA-seq Data with DESeq2. Genome Biology, 15, 550. [PubMed: 25516281]

Ma C, Wei S and Song Y (2011). T790M and acquired resistance of EGFR TKI: a literature review of clinical reports. Journal of Thoracic Disease, 3(1), 10–18. [PubMed: 22263058]

McLaughlin-Drubin ME, Crum CP, and Münger K (2011). Human papillomavirus E7 oncoprotein induces KDM6A and KDM6B histone demethylase expression and causes epigenetic reprogramming. Proceedings of the National Academy of Sciences of the United States of America, 108(5), 2130–2135. [PubMed: 21245294]

Metzeler KH, Maharry K, Radmacher MD, Mrozek K, Margeson D, Becker H, Curfman J, Holland KB, Schwind S, Whitman SP, et al. (2011). Tet2 Mutations Improve the New European LeukemiaNet Risk Classification of Acute Myeloid Leukemia: A Cancer and Leukemia Group B Study. Journal of Clinical Oncology, 1373–1381. [PubMed: 21343549]

Moran-Crusio K, Reavie L, Shih A, Abdel-Wahab O, Ndiaye-Lobry D, Lobry C, Figueroa ME, Vasanthakumar A, Patel J, Zhao X, et al. (2011). Tet2 loss leads to increased hematopoietic stem cell self-renewal and myeloid transformation. Cancer Cell, 20(1), 11–24. [PubMed: 21723200]

Nibourel O, Kosmider O, Cheok M, Boissel N, Renneville A, Philippe N, Dombret H, Dreyfus F, Quesnel B, Geffroy S, et al. (2010). Incidence and prognostic value of Tet2 alterations in de novo acute myeloid leukemia achieving complete remission. Blood, 116(7), 1132–1135. [PubMed: 20489055]

Nishioka C, Ikezoe T, Furihata M, Yang J, Serada S, Naka T, Nobumoto A, Kataoka S, Tsuda M, Udaka K, and Yokoyama A (2013). $CD34^{+}/CD38^{-}$ acute myelogenous leukemia cells aberrantly express CD82 which regulates adhesion and survival of leukemia stem cells. International journal of cancer. Journal International du Cancer, 132(9), 2006–2019. [PubMed: 23055153]

Peters TJ, Buckley MJ, Statham AL, Pidsley R, Samaras K, Lord RV, Clark SJ, Molloy PL (2015). De novo identification of differentially methylated regions in the human genome. Epigenetics & Chromatin, 8, 6. [PubMed: 25972926]

R Core Team (2019). R: A language and environment for statistical computing. R Foundation for Statistical Computing, Vienna, Austria.

Ran D, Shia WJ, Lo MC, Fan JB, Knorr DA, Ferrell PI, Ye Z, Yan M, Cheng L, Kaufman DS, et al. (2013). RUNX1a enhances hematopoietic lineage commitment from human embryonic stem cells and inducible pluripotent stem cells. Blood, 121(15), 2882–2890. [PubMed: 23372166]

Rasmussen KD, Jia G, Johansen JV, Pedersen MT, Rapin N, Bagger FO, Porse BT, Bernard OA, Christensen J, and Helin K (2015). Loss of Tet2 in hematopoietic cells leads to DNA hypermethylation of active enhancers and induction of leukemogenesis. Genes & Development, 29(9), 910–922. [PubMed: 25886910]

Rothenberg-Thurley M, Amler S, Goerlich D, Köhnke T, Konstandin NP, Schneider S, Sauerland MC, Herold T, Hubmann M, Ksienzyk B, et al. (2018). Persistence of preleukemic clones during first remission and risk of relapse in acute myeloid leukemia. Leukemia, 32(7), 1598–1608. [PubMed: 29472724]

Sanchez-Vega F, Mina M, Armenia J, Chatila WK, Luna A, La KC, Dmitriadoy S, Liu DL, Kantheti HS, Saghafinia S, et al. (2018). Oncogenic signaling pathways in The Cancer Genome Atlas. Cell, 173(2), 321–337.e10. [PubMed: 29625050]

Shih AH, Jiang Y, Meydan C, Shank K, Pandey S, Barreyro L, Antony-Debre I, Viale A, Socci N, Sun Y, et al. (2015). Mutational cooperativity linked to combinatorial epigenetic gain of function in acute myeloid leukemia. Cancer Cell, 27(4), 502–515. [PubMed: 25873173]

Smith AE, Mohamedali AM, Kulasekararaj A, Lim Z, Gaken J, Lea NC, Przychodzen B, Mian SA, Nasser EE, Shooter C, et al. (2010). Next-generation sequencing of the Tet2 gene in 355 MDS and CMML patients reveals low-abundance mutant clones with early origins, but indicates no definite prognostic value. Blood, 116(19), 3923–3932. [PubMed: 20693430]

Su Y, Wei W, Robert L, Xue M, Tsoi J, Garcia-Diaz A, Homet Moreno B, Kim J, Ng RH, Lee JW, et al. (2017). Single-cell analysis resolves the cell state transition and signaling dynamics associated with melanoma drug-induced resistance. Proceedings of the National Academy of Sciences of the United States of America, 114(52), 13679–13684. [PubMed: 29229836]

Tian Y, Morris TJ, Webster AP, Yang Z, Beck S, Andrew F, Teschendorff AE (2017). ChAMP: updated methylation analysis pipeline for Illumina BeadChips. Bioinformatics, 33(24), 3982–3984. [PubMed: 28961746]

Tyner JW, Tognon CE, Bottomly D, Wilmot B, Kurtz SE, Savage SL, Long N, Schultz AR, Traer E, Abel M, et al. (2018). Functional genomic landscape of acute myeloid leukaemia. Nature, 562(7728), 526–531. [PubMed: 30333627]

Vagapova ER, Spirin PV, Lebedev TD, & Prassolov VS (2018). The role of TAL1 in hematopoiesis and leukemogenesis. Acta Naturae, 10(1), 15–23. [PubMed: 29713515]

Venables WN & Ripley BD (2002). Modern Applied Statistics with S.

Weissmann S, Alpermann T, Grossmann V, Kowarsch A, Nadarajah N, Eder C, Dicker F, Fasan A, Haferlach C, Haferlach T, Kern W, Schnittger S, & Kohlmann A (2012). Landscape of TET2 mutations in acute myeloid leukemia Leukemia, 26(5), 934–942. Wolfram Research, Inc., Wolfram|Alpha www.wolframalpha.com. (Accessed: 22 September 2019). [PubMed: 22116554]

Xu B, Wang S, Li R, Chen K, He L, Deng M, Kannappan V, Zha J, Dong H, and Wang W (2017). Disulfiram/copper selectively eradicates AML leukemia stem cells in vitro and in vivo by simultaneous induction of ROS-JNK and inhibition of NF-κB and Nrf2. Cell Death & Disease, 8(5), e2797. [PubMed: 28518151]

Yamazaki J, Jelinek J, Lu Y, Cesaroni M, Madzo J, Neumann F, He R, Taby R, Vasanthakumar A, Macrae T, et al. (2015). Tet2 Mutations Affect Non-CpG Island DNA Methylation at Enhancers and Transcription Factor-Binding Sites in Chronic Myelomonocytic Leukemia. Cancer Research, 75(14), 2833–2843. [PubMed: 25972343]

Zeijlemaker W, Grob T, Meijer R, Hanekamp D, Kelder A, Carbaat-Ham JC, Oussoren-Brockhoff YJM, Snel AN, Velhuizen D, Scholten WJ, et al. (2018). CD34+CD38^{-} leukemic stem cell

frequency to predict outcome in acute myeloid leukemia. Leukemia, 33, 1102–1112. [PubMed: 30542144]

Highlights

- TET2 knockout in human AML cell lines increases stem-like signatures
- $TET2^{KO}$ cells have altered dynamics between stem-like/differentiated states
- Altered cell-state switching dynamics provides fitness advantage in and out of drug

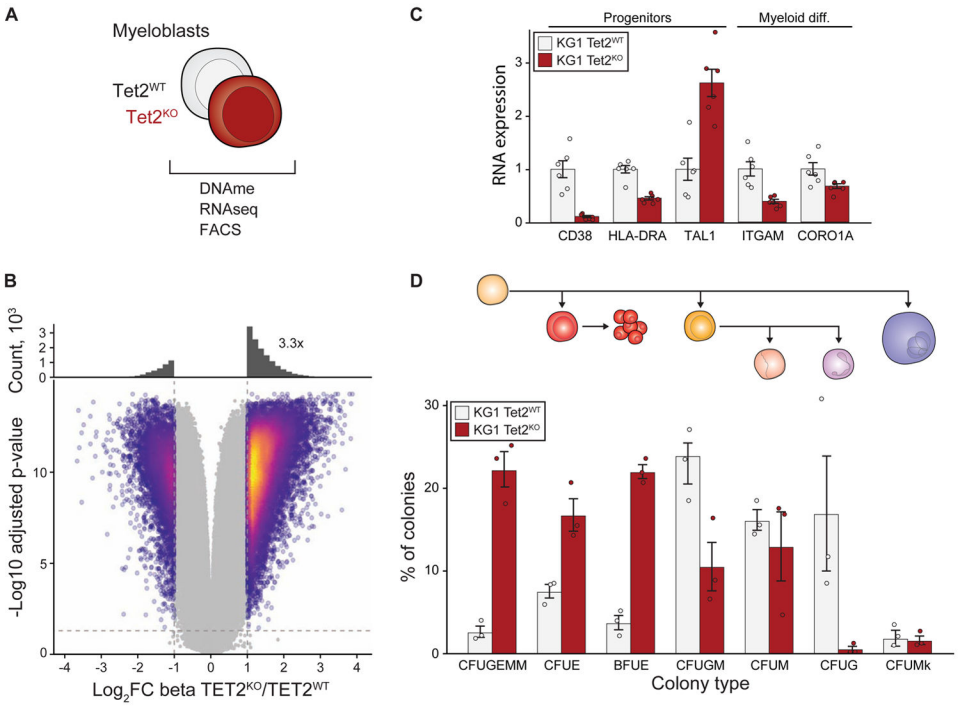

Figure 1. TET2^{KO} cells are more stem-like than TET2^{WT} isogenic counterparts.

(A) Overview of molecular profiling performed on isogenic TET2 mutant AML cell lines. (B) Representative volcano plot and histogram of CpG methylation in TET2^{KO} cells relative to TET2^{WT} (shown for KG1). (C) TET2^{KO} cells show decreased expression of myeloid commitment markers (ITGAM, CORO1A) and increased expression of markers associated with stemness (CD38^{-}, HLA-DRA^{-}, TAL1) compared to TET2^{WT} in both KG1 and Thp1 cells (Supplemental Figure 1B, mean ± s.e., n=6). (D) KG1 and Thp1 (Supplemental Figure 1F) TET2^{KO} cells produce a higher percentage of colonies associated with oligopotent progenitors (CFUGEMM) compared to TET2^{WT} in methylcellulose assays (mean ± s.e., n=3).

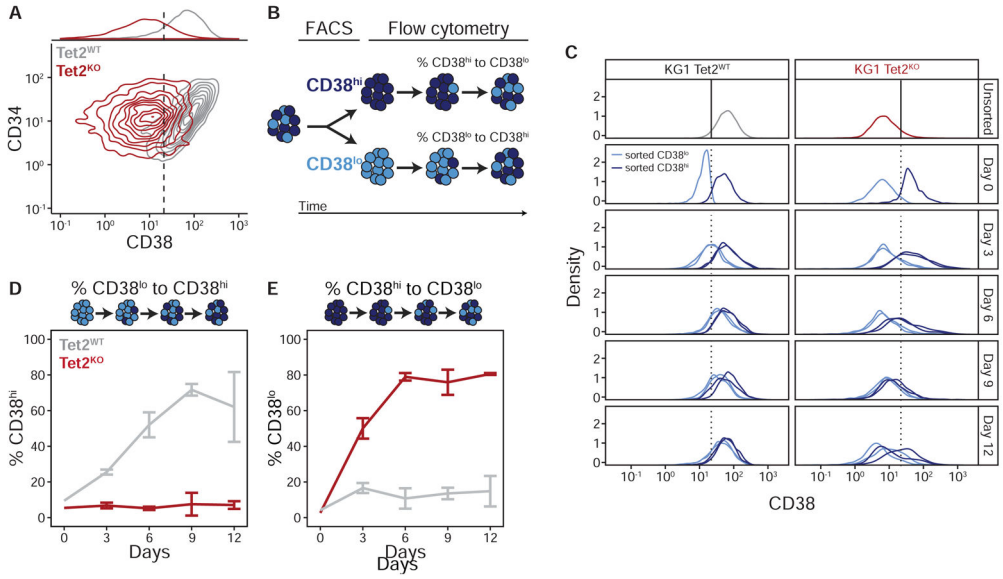

Figure 2. TET2^{KO} increases the propensity of differentiated (CD34^{hi}CD38^{hi}) Cells to switch to a more stem-like (CD34^{hi}CD38^{lo}) cell state.

(A) KG1 TET2^{KO} cell lines show a shift in CD38 surface marker expression. The threshold for calling cells CD38^{lo} or CD38^{hi} (vertical dashed line) is defined by negative controls, such that 99.5% of unstained cells are incorrectly called CD38^{lo} (Supplemental Figure 2A). (B) Schematic illustration of flow cytometry experiment to quantify CD38 expression over time. Cells from either KG1 TET2^{WT} or TET2^{KO} cell lines are sorted by CD38 expression via FACS (fluorescence-activated cell sorting) into CD38^{lo} or CD38^{hi} based on the threshold in (A), and changes in CD38 expression are assessed every 72h by flow cytometry. (C) The distributions of CD38 expression measured by flow cytometry for sorted “lo” or “hi” populations over 12d in 0uM AraC, colored by the original sorted population (n=3). (D-E) Shown is the percent of CD38^{hi} cells in originally pure populations of CD38^{lo} cells (D), or the percent CD38^{lo} cells in originally pure populations of CD38^{hi} cells (E) for KG1 TET2^{WT} and TET2^{KO} cells after 0, 3, 6, 9, and 12 days of growth in drug-free media (mean ± s.e., n=2).

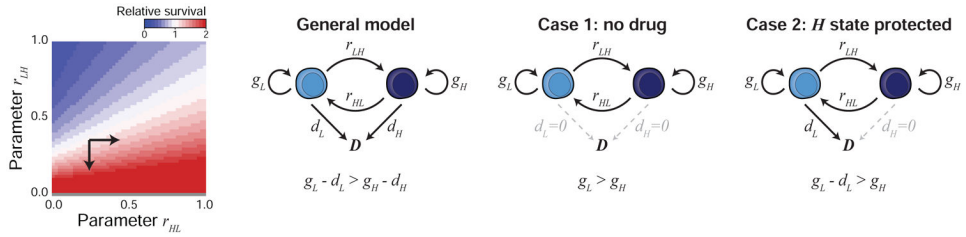

Figure 3. Mathematical model reveals advantageous and disadvantageous parameter regimes for cell-state switching.

(left) If model parameters satisfy Inequality 1, increasing $\boldsymbol{r_{HL}}$ and/or decreasing $\boldsymbol{r_{LH}}$ (black arrows) slows population decay and benefits a drug-treated cancer population. (General model) Schematic representation of mathematical model with two cell states: a stem-cell-like state $\boldsymbol{L}$ and a differentiated state $\boldsymbol{H}$. Parameters $\boldsymbol{d_L}$ and $\boldsymbol{d_H}$ represent the death rates of the $\boldsymbol{L}$ and $\boldsymbol{H}$ states; $\boldsymbol{g_L}$ and $\boldsymbol{g_H}$ the proliferation rates; and $\boldsymbol{r_{LH}}$ and $\boldsymbol{r_{HL}}$ the transition rates from $\boldsymbol{L}$ to $\boldsymbol{H}$ and $\boldsymbol{H}$ to $\boldsymbol{L}$. (Case 1) If cells rarely die ($\boldsymbol{d_L} \approx \boldsymbol{0}$, $\boldsymbol{d_H} \approx \boldsymbol{0}$) and the proliferation rate $\boldsymbol{g_L}$ is higher than $\boldsymbol{g_H}$, increasing $\boldsymbol{r_{HL}}$ is always beneficial. (Case 2) Conversely, if one state were protected from drug effect ($\boldsymbol{d_H} \approx \boldsymbol{0}$), increasing $\boldsymbol{r_{HL}}$ is only beneficial in the unlikely scenario when net production rate of $\boldsymbol{L}$ is larger than the proliferation rate $\boldsymbol{g_H}$.

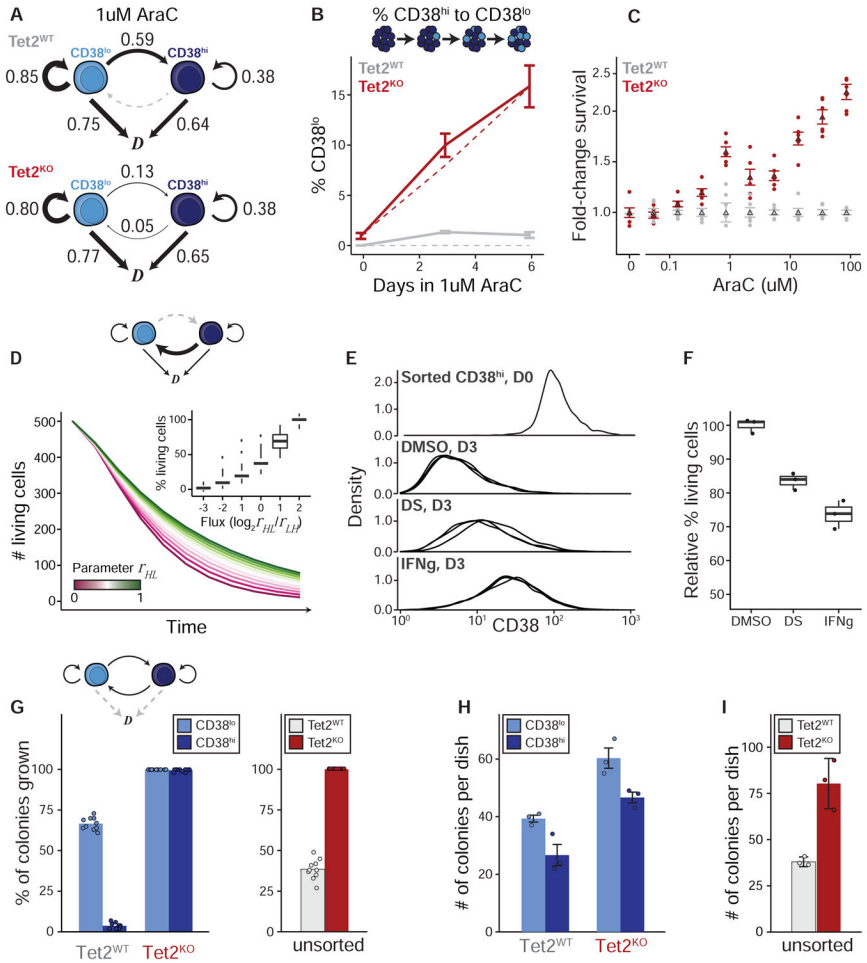

Figure 4. TET2^{KO} cells' altered cell-state dynamics enable longer-term drug survival in chemotherapy.

(A) Schematic illustration of model in 1uM AraC treatment. Numbers are representative estimated rates of transition, proliferation, and death (see Supplemental Figure 3H-I). (B) The percent of KG1 CD38^{lo} cells in originally pure populations of sorted CD38^{hi} cells in 1uM AraC after 0, 3, and 6 days (mean ± s.e., n=3). Dashed lines: predictions from the model. (C) Shown is fold-change cell viability relative to TET2^{WT} cells after 72h exposure to varying concentrations of AraC (mean ± s.e., n=5). (D) Model predictions for drug survival given increasing values of the transition parameter $\boldsymbol{r_{HL}}$ for a toy model that fulfills Inequality 1. Inset: survival as a function of the ratio of $\boldsymbol{r_{HL}/r_{LH}}$. (E-F) TET2^{KO} CD38^{hi} cells were isolated by FACS and incubated with or without effector for 72h in the presence of 1uM AraC. (E) The CD38 distributions after 72h in DMSO, DS, or IFNg treatment (n=3, TET2^{WT} in Supplemental Figure 4A). (F) The percent of living cells in the population relative to control after 72h in DMSO, DS, or IFNg treatment (mean ± s.e., n=3). (G) Model predictions for colony outgrowth from a small population given sorted CD38^{lo} and CD38^{hi} (left) or unsorted cells (right; see Methods, mean of 10 runs). (H) Number of colonies in methylcellulose assays after seeding equal numbers of TET2^{WT} and TET2^{KO} cells (mean ±

s.e., n=3). (I) Number of colonies in methylcellulose assays for cells sorted by CD38 expression (mean ± s.e., n=3).

KEY RESOURCES TABLE

REAGENT or RESOURCE	SOURCE	IDENTIFIER
Antibodies		
PE Mouse anti-Human CD34	BD Biosciences	555822
PE-Cy5 Mouse anti-Human CD38	BD Biosciences	555461
Chemicals, Peptides, and Recombinant Proteins		
Cytosine Beta-D-Arabinofuranoside	Sigma-Aldrich	C6645
Disulfiram	Sigma-Aldrich	D2950000
Human IFN-g	PeproTech	300-02
Critical Commercial Assays		
CellTiter-Glo 2.0 Cell Viability Assay	Promega	G9242
QuantSeq 3’ mRNA-Seq Library Prep Kit FWD for Illumina	Lexogen	0.15.24/96
MethoCult H4034 Optimum	STEMCELL	#04034
Deposited Data		
Raw and analyzed data	This paper; Mendeley data	doi:10.17632/xmvz47rpg6.1
Epigenome analysis of leukemia stem, blast and normal hematopoietic stem/progenitor cells	Jung et al., 2015; GEO	GSE63409
Experimental Models: Cell Lines		
Human male: KG-1	ATCC	CCL-246; RRID: CVCL_0374
Human male: THP-1	ATCC	TIB-202; RRID: CVCL_0006
Oligonucleotides		
Primer HOXA5-F: TCTCGTTGCCCTAATTCATCTTTT	McLaughlin-Drubin et al., 2011	N/A
Primer HOXA5-R: CATTCAGGACAAAGAGATGAACAGA	McLaughlin-Drubin et al., 2011	N/A
Primer CD38-F: CACCAAGCGCTTTCCCGAGACC	This paper	N/A
Primer CD38-R: GAGAGGCCCCTCCAGTGCAGAA	This paper	N/A
Primer CORO1A-F: GTGGTCCGCTCCAGCAAGTTCC	This paper	N/A
Primer CORO1A-R: CAGACCGTGGGCGCATTCTTGT	This paper	N/A
Primer ITGAM-F: CTCCGTGGACGTGGACAGCAAC	This paper	N/A
Primer ITGAM-R: AATGGCCACGTCCGTCAGCTTG	This paper	N/A
Primer TAL1-F: GGGAGCCGGATGCCTTCCCTAT	This paper	N/A
Primer TAL1-R: ACTTCATGGCCAGGCGGAGGAT	This paper	N/A
Recombinant DNA		
pSpCas9(BB)-2A-Puro (PX459) V2.0	Addgene	#62988
Software and Algorithms		

REAGENT or RESOURCE	SOURCE	IDENTIFIER
Code to generate all figures	This paper; Mendeley data	doi:10.17632/xmvz47rpg6.1
Code pertaining to model	This paper; GitHub	https://github.com/AltschulerWu-Lab/tet2-dynamics
DNA methylation age calculator	Horvath, 2013	https://horvath.genetics.ucla.edu/html/dnamage/
R	R Core Team, 2019	https://www.R-project.org
MATLAB	R2019a	https://www.mathworks.com